[CANCER RESEARCH 64, 4227–4234, June 15, 2004]

Position in Cell Cycle Controls the Sensitivity of Colon Cancer Cells to Nitric Oxide-Dependent Programmed Cell Death

Anne Jarry,[1] Laetitia Charrier,[1] Chantal Bou-Hanna,[1] Marie-Claire Devilder,[2] Véronique Crussaire,[1] Marc G. Denis,[1] Geneviève Vallette,[1] and Christian L. Laboisse[1,3]

[1]Institut National de la Santé et de la Recherche Médicale U539, Faculté de Médecine, Nantes, France, and [2]Institut National de la Santé et de la Recherche Médicale U463 and [3]Pathology Department, University Hospital, Nantes, France

ABSTRACT

Mounting evidence suggests that the position in the cell cycle of cells exposed to an oxidative stress could determine their survival or apoptotic cell death. This study aimed at determining whether nitric oxide (NO)-induced cell death in colon cancer cells might depend on their position in the cell cycle, based on a clone of the cancer cell line HT29 exposed to an NO donor, in combination with the manipulation of the cell entry into the cell cycle. We show that PAPA NONOate (pNO), from 10^{-4} M to 10^{-3} M, exerted early and reversible cytostatic effects through ribonucleotide reductase inhibition, followed by late resumption of cell growth at 5×10^{-4} M pNO. In contrast, 10^{-3} M pNO led to late programmed cell death that was accounted for by the progression of cells into the cell cycle as shown by (*a*) the accumulation of apoptotic cells in the G_2-M phase at 10^{-3} M pNO treatment; and (*b*) the prevention of cell death by inhibiting the entry of cells into the cell cycle. The entry of pNO-treated cells into the G_2-M phase was associated with actin depolymerization and its *S*-glutathionylation in the same way as in control cells. However, the pNO treatment interfered with the build-up of a high reducing power, associated in control cells with a dramatic increase in reduced glutathione biosynthesis in the G_2-M phase. This oxidative stress prevented the exit from the G_2-M phase, which requires a high reducing power for actin deglutathionylation and its repolymerization. Finally, our demonstration that programmed cell death occurred through a caspase-independent pathway is in line with the context of a nitrosative/oxidative stress. In conclusion, this work, which deciphers the connection between the position of colonic cancer cells in the cell cycle and their sensitivity to NO-induced stress and their programmed cell death, could help optimize anticancer protocols based on NO-donating compounds.

INTRODUCTION

It is becoming increasingly clear that nitric oxide (NO)-releasing agents can exert antitumor effects through the antiproliferative, cytotoxic, and apoptotic effects of NO (1–5). It has been reported that NO-induced early cytostasis begins with a rapid and reversible inhibition of the ribonucleotide-reductase enzyme, which is the first, rate-limiting step in the production of deoxynucleoside triphosphates required for cell replication and DNA repair (1, 6, 7). Deleterious effects of NO are likely caused by a unique NO chemistry at high NO concentration in biological media. NO undergoes autoxidation and forms reactive nitrogen species that support a nitrosation/oxidation chemistry leading to cell injury and cell death (8).

Recent evidence has suggested that cell cycle and oxidative stress may be team players in triggering cell death (9). In particular, the position in the cell cycle of cells exposed to an oxidative stress could determine their survival or their apoptotic cell death (10, 11). These recent studies raise the important issue of whether the cell death of tumor cells exposed to NO may depend on where the cell resides in the cell cycle.

In this study, based on a differentiated clonal derivative (12) of the human colonic cancer cell line HT29 (13) largely used for deciphering the mechanisms of colon cancer apoptosis (4, 14–19), we show for the first time a connection between the position of human cancer cells in the cell cycle and their sensitivity to NO-induced programmed cell death. We show a dual effect of NO. Whatever its concentration, NO exerted early and reversible cytostatic effects, followed by resumption of progression into the cell cycle. Interestingly, at a sufficiently high concentration of NO, the reentry of cancer cells into the cell cycle triggered their apoptotic cell death in the G_2-M phase. The mechanism leading to cell death involves a shift toward an oxidized redox status, as demonstrated by the evaluation of the glutathione redox status and the demonstration of a caspase-independent cell death.

MATERIALS AND METHODS

Cell Culture and Treatment. The HT29-Cl.16E cell line (12), a clonal derivative of the HT29 cell line (13), is a well-characterized, polarized epithelial cell line (20–23). HT29-Cl.16E cells were routinely cultured in DMEM/10% (v/v) FCS (both from Life Technologies, Rockville, MD). Cells were tested for *Mycoplasma* contamination every 2 months and were always confirmed *Mycoplasma* negative using the Hoechst 33258 test (Calbiochem, San Diego, CA). For the experiments, HT29-Cl.16E cells were seeded at 40×10^3 cells/ml in 5 ml DMEM/10% FCS in six-well culture plates (Costar, Cambridge, MA). Three days after seeding, the medium was discarded and replaced by 1 ml DMEM/10% FCS. If not otherwise specified, the cells were used during the exponential phase of growth, which is characterized by cells growing in clusters. Cells were treated with the NO donor PAPA NONOate (pNO; Cayman, Spi Bio, Massy, France) at the indicated concentrations and time periods. Decomposition of pNO in NO was followed spectrophotometrically at 250 nm as described in the manufacturer's instructions. Decomposition was achieved within 45-min incubation in the culture medium at 37°C (data not shown). In some experiments, PD98059 (Alexis, Coger S.A., Paris, France), an inhibitor of the extracellular signal-regulated kinase 1/2 subclass of mitogen-activated protein kinases, was added to the culture medium at the indicated concentrations 1 h before pNO addition. After a 24-h or 48-h pNO treatment, adherent cells and floating cells were collected. For some experiments, HT29-Cl.16E cells were exposed to the combination of human activating anti-Fas antibody (10 ng/ml, clone CH-11; Upstate Biotechnology, Lake Placid, NY), IFN-γ (10 ng/ml; R&D Systems, Minneapolis, MN), and Adriamycin (Sigma, St. Louis, MO) as described previously (18). This treatment is referred to as IFA throughout the text.

Mitotic Detachment. HT29-Cl.16E cells were plated in 75-cm^2 flasks at 9×10^6 cells/flask. Two days later, mitotic cells were collected by vigorous shaking, centrifuged, and either collected for the measurement of glutathione content or cytospun on coverslips for immunofluorescence followed by confocal microscopy analysis. To verify that most of the cells were in the G_2-M phase of the cell cycle, a cyclin B1 antibody was used (see "Confocal Microscopy"). Remaining adherent cells were collected after scraping in PBS with a rubber policeman, and centrifuged; the glutathione content then was assessed. Adherent cells also were used for immunofluorescence and confocal microscopy analysis after trypsinization and cytospin preparations on coverslips.

Received 1/26/04; revised 3/22/04; accepted 4/5/04.

Grant support: Ligue Départementale de Loire-Atlantique Contre le Cancer. L.Charrier is the recipient of a fellowship from the Ligue Départementale de Vendée Contre le Cancer.

The costs of publication of this article were defrayed in part by the payment of page charges. This article must therefore be hereby marked *advertisement* in accordance with 18 U.S.C. Section 1734 solely to indicate this fact.

Note: A. Jarry and L. Charrier contributed equally to the work.

Requests for reprints: C. L. Laboisse, INSERM U539, Faculté de Médecine, 1 Rue Gaston Veil, 44035 Nantes cedex 01, France. Phone: 33-240-41-28-30; Fax: 33-240-41-28-37; E-mail: laboisse@sante.univ-nantes.fr.

Cell Culture for Immunoblot and DNA Fragmentation Analysis. HT29-Cl.16E cells were seeded at 40×10^3 cells/ml in 30 ml DMEM/FCS in 10-cm-diameter Petri dishes (Costar). After 3 days of culture, the medium was discarded and replaced by 6 ml DMEM/FCS, and cells were submitted to a cytotoxic treatment as described previously.

Cell Proliferation Assay. Cell proliferation was measured by [^{3}H]-thymidine incorporation. HT29-Cl.16E cells, cultured in six-well plates, were treated for 1 h with increasing concentrations of pNO and then pulsed for 4 h with [^{3}H]-thymidine (2 μCi/ml; Amersham, Piscataway, NJ). Radioactivity incorporated into the DNA was measured as described previously (24). For some experiments, increasing concentrations of adenosine, guanosine (0–500 μM each), and 0.5 μM cytidine (all from Sigma) were added concomitantly with [^{3}H]-thymidine.

Cell Viability Assay. After a 24-h or 48-h pNO (10^{-3} M) treatment, floating cells and adherent cells, detached by trypsinization, were counted in a hemacytometer. Percent cell growth relative to time point 0 was defined as (adherent cells at time point 24 h or 48 h/adherent cells at time point 0) $\times$ 100. Percent cell loss relative to time point 0 was defined as (floating cells at time point 24 h or 48 h/adherent cells at time point 0) $\times$ 100. When the cells were pretreated with 50 μM PD98059 and then exposed to 10^{-3} M pNO for 48 h, floating and adherent cells were counted. Percent floating cells was expressed as [floating cells/(floating cells + adherent cells)] $\times$ 100.

Hoechst Staining. The DNA-specific dye Hoechst 33258 (Calbiochem), 0.5 μg/ml in Hank's balanced sodium salt without phenol red (Life Technologies, Inc.), was used on Carnoy-fixed cytocentrifuged preparations of cells.

Ultrastructural Studies. HT29-Cl.16E cells were harvested and centrifuged at 100 $\times$ *g*. The cell pellets were fixed in 3% glutaraldehyde in cacodylate buffer and prepared for electron microscopy by standard methods.

Cell Cycle Analysis by Flow Cytometry. HT29-Cl.16E cells were cultured in six-well culture plates and submitted to a 48-h pNO treatment in the presence or absence of 50 μM PD98059. After gentle rinsing of the monolayers with PBS, floating cells or trypsinized cells from the monolayer were washed with PBS, centrifuged at 1500 rpm for 10 min, and resuspended in a propidium iodide-staining solution (40 μg/ml propidium iodide in 0.1% sodium citrate, 0.1% Triton X-100, and 20 μg/ml RNase A) for 30 min in the dark. Cell cycle profile of no less than 20,000 cells was generated on a FACS Calibur flow cytometer (Becton Dickinson, San Jose, CA). Data were collected with the Cell Quest Pro software (Becton Dickinson) and analyzed using Modfit LT software (Verity Software, Topsham, ME).

Confocal Microscopy. HT29-Cl.16E cells, cultured on glass coverslips in six-well culture plates and submitted to a 48-h pNO treatment, were fixed *in situ* in 4% paraformaldehyde in PBS buffer for 15 min and washed in PBS (3 $\times$ 5 min). Glutathione was detected in adherent cells on coverslips and on cytospin preparations of floating apoptotic cells using the following protocol. Cells were preincubated for 30 min with PBS/0.1% Triton X-100/4% horse serum and exposed for 1 h to a monoclonal antibody directed to glutathione (1:50; Virogen, Watertown, MA). After washing, cells were incubated for 30 min at room temperature with Alexa fluor 488-conjugated goat antimouse antibody (1:100; Molecular Probes, Eugene, OR) in PBS/0.1% Triton X-100/4% horse serum. Under the fixation procedure (paraformaldehyde), free reduced glutathione (GSH) was washed out. To verify the specificity of PrSSG labeling with the anti-GSH antibody, the fixed cells were treated for 30 min with 10 mM DTT (Sigma) before labeling with the anti-GSH antibody. As expected from a treatment that reduces the disulfide-bounded cysteine residues, DTT pretreatment prevented any labeling with the anti-GSH antibody.

Cyclin B1 was detected in floating and adherent pNO-treated cells using a monoclonal antibody (1:20; Novocastra, Newcastle upon Tyne, UK) with the same protocol as described previously.

For F-actin and G-actin detection, floating and adherent cells were fixed and preincubated in PBS/4% horse serum/0.1% Triton X-100 as mentioned previously. Cells then were stained for 30 min at room temperature in the dark with phalloidin conjugated to Alexa fluor 488 (2 units/coverslip; Molecular Probes) for the detection of F-actin, and/or with DNase I conjugated to Texas red (0.3 μM; Molecular Probes) for the detection of G-actin. For double labeling of GSH and G-actin, anti-GSH antibody was first applied, followed by the Alexa fluor 488-conjugated goat antimouse antibody. After washing with PBS, coverslips then were incubated with DNase I conjugated to Texas red and washed with PBS.

All of the coverslips were mounted using Prolong antifade medium (Molecular Probes). Imaging was performed on a Leica TCS-SP1 confocal laser-scanning microscope (Leica, Heidelberg, Germany) equipped with an argon/krypton laser. Cells were visualized with a 63×/1.4 NA oil objective lens. Image processing was performed using TCS-NT software (Leica).

Immunoblot Analysis. Whole cell lysates were prepared in a stringent SDS-containing RIPA buffer as described previously (18). Briefly, cells were lysed for at least 30 min on ice in a lysis buffer containing 150 mM NaCl, 0.5% deoxycholate, 50 mM Tris-HCl (pH 8.0), and 0.1% SDS, supplemented with protease inhibitors 0.1 mM Pefabloc (Roche Diagnostics, Meylan, France), 2.5 μg/ml pepstatin, 10 μg/ml aprotinin, and 5 μg/ml leupeptin. Protein concentrations were determined using the Folin assay (DC protein assay kit; Bio-Rad, Hercules, CA). The protein-containing lysate was mixed with 2× loading buffer and run on 10% SDS-polyacrylamide gels. Proteins were electrotransferred onto nitrocellulose membranes (Bio-Rad) using a *trans*-blot apparatus (Bio-Rad). After an overnight blocking (1% blocking reagent; Roche Diagnostics), the membranes then were probed with rabbit polyclonal antibodies directed either to human caspase-3 (1:2500; PharMingen, San Diego, CA) or to human ICAD (1:500; PharMingen), followed by horseradish peroxidase-conjugated goat antirabbit antibody (1:10,000; Jackson ImmunoResearch, West Grove, PA). For the detection of glutathionylated proteins, an anti-GSH monoclonal antibody (1:500; Virogen) was used, followed by horseradish peroxidase-conjugated goat antimouse antibody (1:1000; Santa Cruz Biotechnology, Santa Cruz, CA). The immunoreactive proteins were detected on films using an enhanced chemiluminescence substrate according to the manufacturer's instructions (Roche Diagnostics).

Measurement of Intracellular Glutathione Content. Intracellular GSH and oxidized glutathione (GSSG) levels were determined using an enzymatic recycling method described by Tietze (25) and modified by Baker *et al.* (26). Briefly, floating cells and adherent cells harvested by scraping with a rubber policeman in PBS without Ca^{2+} and Mg^{2+} were sonicated at 0°C and incubated for 15 min at 0°C with 5% sulfosalicylic acid to reach a final concentration of 1% sulfosalicylic acid (1:4; v/v). The mixture was centrifuged at 15,000 $\times$ *g* for 10 min at 4°C. The pellet was solubilized in 1 M NaOH, and its protein content was assayed using the Bradford method (Bio-Rad protein assay kit). The supernatants were stored at −70°C until analysis for GSH and GSSG content, using the GSH disulphide reductase/5,5′-dithiobis-(2-nitrobenzoic acid) recycling method. Results were expressed as nmol of GSH/mg of protein.

Analysis of DNA Fragmentation by Conventional Agarose Gel Electrophoresis. DNA was extracted as described previously (18). Ten μg DNA were analyzed in ethidium bromide-containing 2% agarose precast gels (Invitrogen, Carlsbad, CA).

Analysis of DNA Fragmentation by Pulse-Field Gel Electrophoresis. After pNO treatment, floating HT29-Cl.16E or adherent cells harvested by trypsinization were washed with PBS (without Ca^{2+} and Mg^{2+}) and suspended in PBS (without Ca^{2+} and Mg^{2+}) containing 5 mM EDTA. To this cell suspension was added an equal volume of 1.5% low melting agarose in PBS containing 5 mM EDTA as described previously (27). The resulting 0.75% agarose plugs were solidified at 4°C for 30 min and incubated 1 h at 37°C in lysis buffer [50 mM NaCl, 20 mM Tris-HCl (pH 8.0), 20 mM EDTA, 0.5% laurylsarcosine, 50 μg/ml RNase A, and 100 μg/ml proteinase K]. Plugs then were washed three times in washing buffer [20 mM Tris-HCl (pH 8.0) and 20 mM EDTA]. Agarose plug pieces, each containing 0.5×10^6 cells, were loaded into a 1% agarose gel and run in 0.5× Tris-borate EDTA for 16 h using the CHEF-DR III electrophoresis cell (Bio-Rad). Running conditions were as follows: 15°C temperature, 50–90 s switch time, 120° angle, and 6 V/cm voltage gradient. DNA size standard (0.05–1 Mb) was Lambda Ladder (Bio-Rad). Gels were stained in 0.5× Tris-borate EDTA with ethidium bromide (0.8 μg/ml) for 30 min.

Immunohistochemistry. For immunohistochemistry, HT29-Cl.16E cells were seeded at 50×10^3 cells/ml in DMEM/FCS in four-well Lab-Tek chambers (Merck-Eurolab, Strasbourg, France). After 3 days of culture, the medium was discarded and replaced by 0.5 ml DMEM/FCS, and cells were treated as described previously. Adherent cells and cytocentrifuged preparations of floating cells were stained with the M30 monoclonal antibody (1:50; Roche Diagnostics) as described previously (18). This antibody specifically recognizes a cytokeratin 18 neo-epitope that becomes available at an early caspase cleavage event during apoptosis and can be considered as an early marker of apoptosis in epithelial cells (28).

RESULTS

pNO-Induced Early Antiproliferative Effect. As shown in Fig. 1*A*, pNO dose-dependently inhibited [^{3}H]-thymidine incorporation into DNA during a 5-h incubation. The inhibitory effects of pNO were significant from 10^{-4} M and maximal at 10^{-3} M. The addition of deoxyribonucleosides led to a nearly complete recovery of DNA synthesis in a dose-dependent manner (Fig. 1*B*). Therefore, these early antiproliferative effects of pNO were ascribed to the inhibition of the redox-sensitive enzyme ribonucleotide reductase.

pNO-Induced Late Programmed Cell Death. We then tested the effects of exposure to pNO for 24 h or 48 h. At 24 h, pNO induced a dramatic cytostatic effect without cell loss whatever the pNO concentration used. When the exposure to pNO was prolonged to 48 h, the biological effects were dependent on pNO concentration. At 5×10^{-4} M, cell proliferation resumed without any cytotoxic effect. In contrast, at 10^{-3} M, pNO caused cell rounding mainly at the periphery of cell clusters (Fig. 4*B*, phase contrast microscopy), followed by cell detachment and cell loss into the medium (Fig. 2). Cells exposed to the NO donor allowed to decompose for 2–4 h at 37°C in a cell-free medium beforehand did not undergo cell detachment, thus showing that this effect was specifically related to NO. As shown in Fig. 3*A*, floating pNO-treated cells exhibited typical morphologic features of apoptosis, as assessed by Hoechst staining and electron microscopy. These features include nuclear shrinkage, chromatin condensation, and fragmentation (Fig. 3*A*). These features also were associated with numerous mitotic figures. The pNO-treated adherent cells did not display these features of programmed cell death (Fig. 3*B*).

Apoptotic Cells on pNO Treatment Accumulate in the G_2-M Phase of the Cell Cycle. Our observation of cell rounding together with the numerous mitotic figures observed in floating cells led us to postulate that the apoptotic process was associated with an entry in cell division. To test this hypothesis, we first assessed the distribution in the cell cycle of adherent and floating cells by using flow cytometry after propidium iodide staining. After a 48-h 10^{-3} M pNO treatment, the majority of floating cells accumulated in the G_2-M phase (Fig. 4*A*, *top*), whereas the adherent cells were equally distributed between the G_0-G_1 and S+G_2-M phases of the cell cycle (Fig. 4*B*, *top*).

We then performed an immunohistochemical analysis of cyclin B1 expression, a well-known marker of the G_2-M transition (29). Immunofluorescence followed by laser confocal imaging of floating HT29-Cl.16E cells after a 48-h 10^{-3} M pNO treatment showed that the majority of floating cells were stained with the anticyclin B1 antibody (Fig. 4*A*, *bottom*), with a variable staining intensity. Only a minority of cells scored negative with anticyclin B1 antibody. In addition, the rounded cells at the periphery of the clusters displayed a strong cyclin B1 staining (Fig. 4*B*, *bottom*). These results led to the hypothesis that cell rounding is associated with an entry of cells into mitosis and that cell detachment and cell death are linked to the inability of cells to undergo a complete cell cycle.

Blocking Reentry into the Cell Cycle Prevents NO-Induced Cell Death. As shown in Fig. 5*A*, preincubation of HT29-Cl.16E cells with PD98059 prevented the entire series of events leading to cell

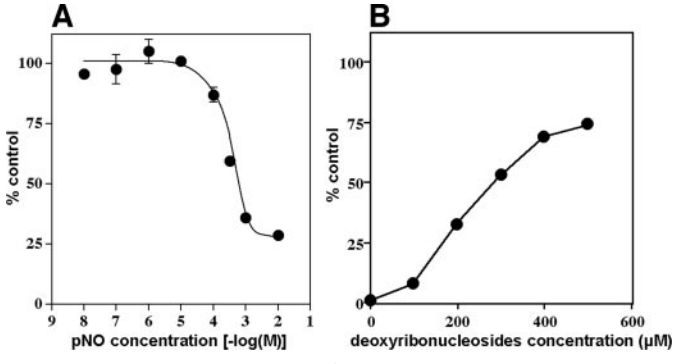

Fig. 1. Effects of nitric oxide (NO) on [^{3}H]-thymidine incorporation in HT29-Cl.16E cells. *A*, HT29-Cl.16E cells were incubated with increasing concentrations of PAPA NONOate (pNO) for 1 h and then pulsed with [^{3}H]-thymidine (2 μCi/ml) as described in "Materials and Methods." *B*, HT29-Cl.16E cells were treated with 10^{-3} M pNO for 1 h and pulsed with [^{3}H]-thymidine (2 μCi/ml) in the presence of increasing concentrations of deoxyribonucleosides as described in "Materials and Methods." Results are expressed as percentage of [^{3}H]-thymidine incorporation of control cells; mean ± SE of three to six determinations.

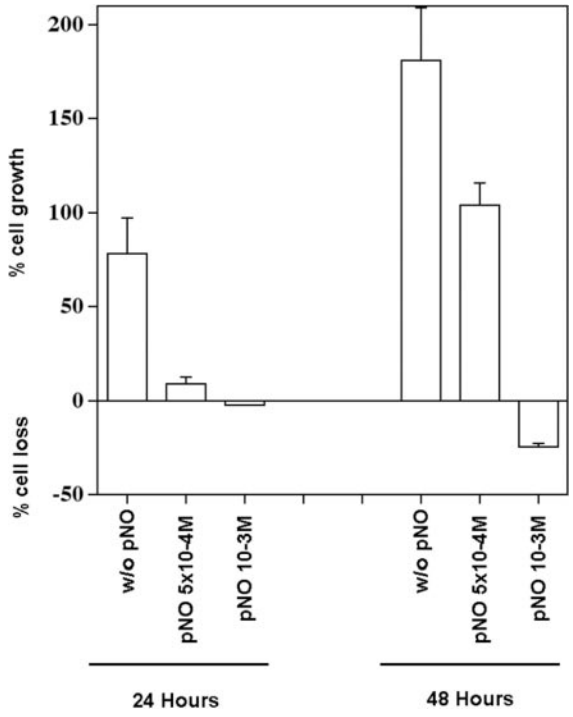

Fig. 2. Nitric oxide (NO)-dependent cytostasis and cell death. HT29-Cl.16E cells were incubated for 24 h or 48 h with or without 5×10^{-4} M or 10^{-3} M PAPA NONOate (*pNO*). Floating cells and adherent cells were collected and counted in a hemacytometer. Percent cell growth and percent cell loss were expressed as described in "Materials and Methods;" mean ± SE of six to nine determinations.

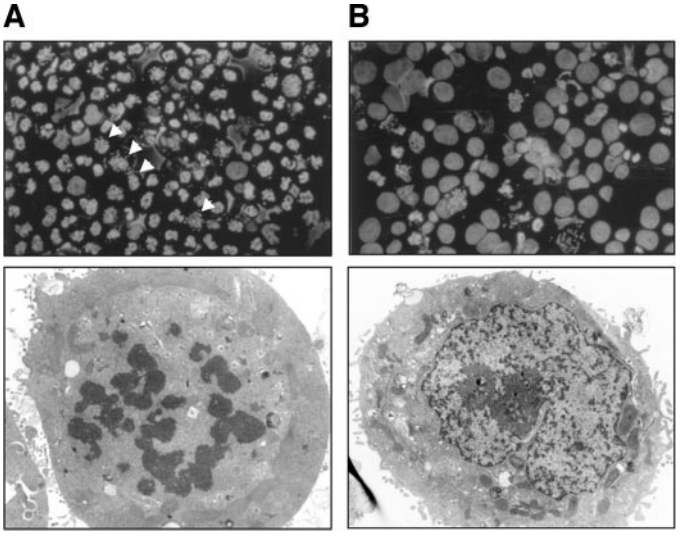

Fig. 3. Morphologic characterization of cell death in PAPA NONOate (pNO)-treated HT29-Cl.16E cells. HT29-Cl.16E cells were exposed to 10^{-3} M pNO for 48 h. Floating (*A*) and adherent (*B*) cells were collected, cytocentrifuged, and stained with Hoechst 33258 dye (*top*; original magnification, ×400) or processed for electron microscopy (*bottom*; original magnification, ×5000). Arrowheads indicate mitotic figures.

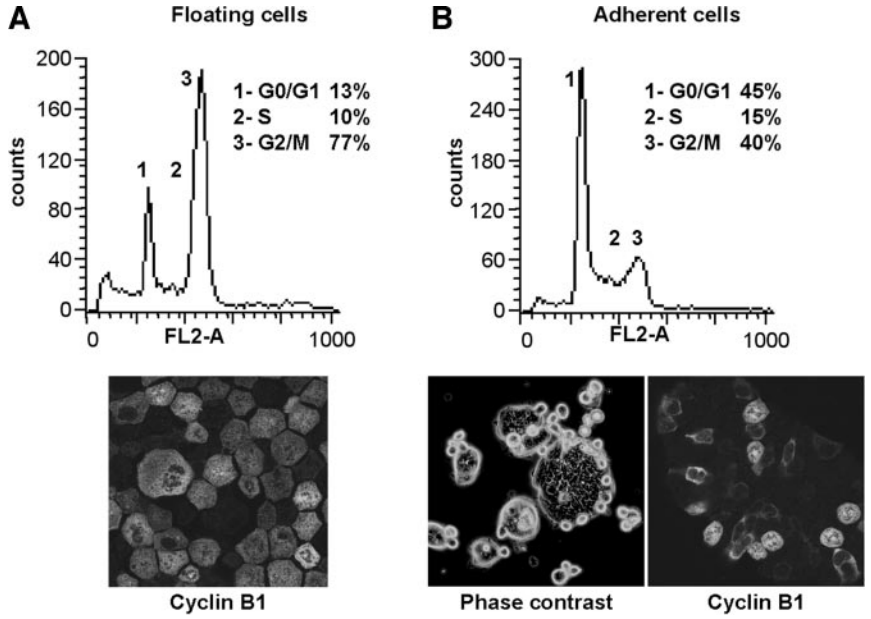

Fig. 4. Characterization of the various phases of the cell cycle in PAPA NONOate (pNO)-treated HT29-Cl.16E cells. Flow cytometry (*top*), HT29-Cl.16E cells were exposed to 10^{-3} M pNO for 48 h. Floating cells (*A*), and trypsinized adherent cells (*B*) were collected, cytocentrifuged, stained with propidium iodide, and examined with a flow cytometer. Percentage of cells in each phase of the cell cycle was calculated using the Modfit LT software. Cyclin B1 staining (*bottom*), HT29-Cl.16E cells, cultured on glass coverslips, were exposed to 10^{-3} M pNO for 48 h. After gentle washing with PBS, adherent cells and cytospun floating cells were fixed with paraformaldehyde, processed for staining with the anticyclin B1 antibody as described in "Materials and Methods," and examined with a confocal microscope. Floating cells (*A*) exhibited a strong staining with the anticyclin B1 antibody, and numerous figures of mitosis can be seen. Rounded cells undergoing detachment mainly at the periphery of the clusters (*B*, phase contrast) were strongly stained with the anticyclin B1 antibody, showing that these cells accumulated in the G_2-M phase.

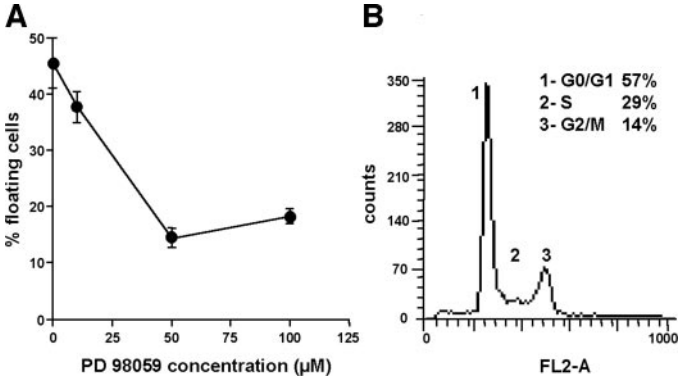

Fig. 5. Inhibitory effect of PD98059 on nitric oxide (NO)-induced cell death. *A*, HT29-Cl.16E cells were pretreated for 1 h with increasing concentrations of PD98059 and exposed to 10^{-3} M PAPA NONOate (pNO) for 48 h. Floating cells and adherent cells were collected and counted in a hemacytometer. Percent floating cells was expressed as: [floating cells/(floating cells + adherent cells)] × 100; mean ± SE of three to nine determinations. *B*, cell cycle profile of cells treated with 10^{-3} M pNO and 50 μM PD98059 for 48 h, trypsinized, and stained with propidium iodide.

death (*i.e.*, cell rounding and cell detachment) on 10^{-3} M pNO treatment. Flow cytometric analysis showed that most of the cells were kept in the G_0-G_1 phase (Fig. 5*B*). Thus, it was concluded that PD98059 protected the cells through its antiproliferative effect.

Fully differentiated postconfluent monolayers of HT29-Cl.16E cells, which are in the G_0-G_1 phase as shown by flow cytometry, also were found to be totally resistant to pNO treatment (data not shown).

Together, these results support the conclusion that the apoptotic effects induced by high NO concentrations are paradoxically associated with a reentry in cell proliferation following the phase of cytostasis.

We then were prompted to examine the glutathione redox status in relation with the cytoarchitectural changes associated with cell rounding and cell death.

G_2-M-Related Redox Changes and Actin Reorganization in HT29-Cl.16E Cells. Because NO is known to react with glutathione, we examined the three forms of glutathione: GSH, GSSG, and glutathionylated proteins.

pNO-Treated Cells. We first examined the pattern of protein *S*-glutathionylation using a monoclonal anti-GSH antibody. Immunoblot analysis of whole cell lysates showed a glutathionylation of an M_r 42,000 protein, likely to be actin, only in floating apoptotic cells (Fig. 6*A*, *Lane 3*). Probing of the membrane with an antiactin antibody revealed that the actin content was identical in the three conditions: control, adherent pNO-treated cells, and floating pNO-treated cells (Fig. 6*C*).

We then evaluated the influence of actin glutathionylation on the balance between F- and G-actin using a morphologic approach. To this end, confocal microscopy was performed on floating and adherent cells after a 48-h treatment with 10^{-3} M pNO using an anti-GSH antibody and labeled phalloidin or DNase I, specific for F- or G-actin, respectively. In floating cells, F-actin persisted as a cortical ring, but the organization in stress fibers was totally lost (Fig. 7, *top*). Actin was depolymerized into G-actin, which underwent *S*-glutathionylation as shown by the overlay of staining when double labeling with anti-GSH and DNase I was performed (Fig. 7, *bottom*). In adherent cells, sectional images of cell clusters at the bottom (Fig. 8, *top*, *left*) showed

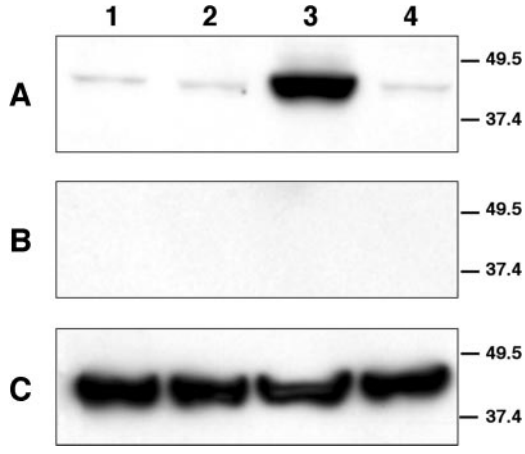

Fig. 6. Glutathionylation of an M_r 42,000 protein on nitric oxide (NO) treatment. HT29-Cl.16E cells were exposed to 10^{-3} M PAPA NONOate (pNO) treatment for 48 h. Lysates obtained from control (*Lane 1*), adherent pNO-treated cells (*Lane 2*), floating pNO-treated cells (*Lane 3*), and adherent pNO-treated cells in the presence of 50 μM PD98059 (*Lane 4*) were submitted to SDS-PAGE electrophoresis in nonreducing conditions (*A*) and reducing conditions (*B* and *C*) and immunoblotted with an anti-reduced glutathione antibody (*A* and *B*) or an anti-β-actin antibody (*C*) as described in "Materials and Methods." Numbers on the right indicate molecular size of standards in kDa.

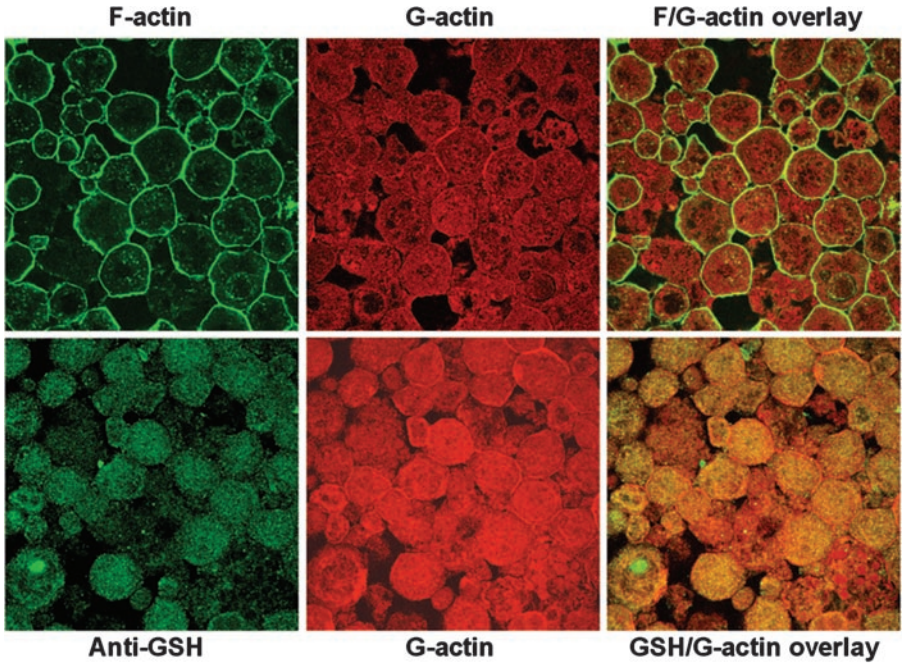

Fig. 7. Assessment by confocal microscopy of depolymerization and *S*-glutathionylation of actin on PAPA NONOate (pNO) treatment in floating cells. HT29-Cl.16E cells, cultured on glass coverslips, were submitted for 48 h to pNO (10^{-3} M) treatment. Floating cells were collected, fixed, and stained with Alexa 488-phalloidin (F-actin) or Texas red DNase I (G-actin) or with an anti-reduced glutathione (*GSH*) antibody as described in "Materials and Methods" and examined by confocal microscopy. *Top*, stress fibers were totally disrupted, and actin was depolymerized into G-actin. *Bottom*, G-actin underwent a *S*-glutathionylation, as shown by the overlay of stainings with an anti-GSH antibody and with Texas red DNase.

a normal stress fiber pattern of F-actin. Only rounded cells undergoing cell detachment at the top of the clusters showed depolymerized G-actin without stress fibers (Fig. 8, *top*, *right*). Interestingly, only those cells undergoing detachment at the top of the clusters were labeled with an anti-GSH antibody (Fig. 8, *bottom*).

Finally, we examined the glutathione redox status of pNO-treated cells, both adherent and floating. As shown in Table 1, floating cells exhibited a dramatic increase in GSH content compared with adherent cells. However, because of an NO-induced oxidation of GSH into GSSG in floating cells, the ratio GSH:GSSG (8.65 ± 0.18) was far less than that of G_2-M control cells (30.98 ± 1.60).

Control G_2-M Cells. When G_2-M HT29-Cl.16E cells were isolated by mitotic detachment, a pattern of depolymerized G-actin was observed that was undistinguishable from that of the G_2-M arrested

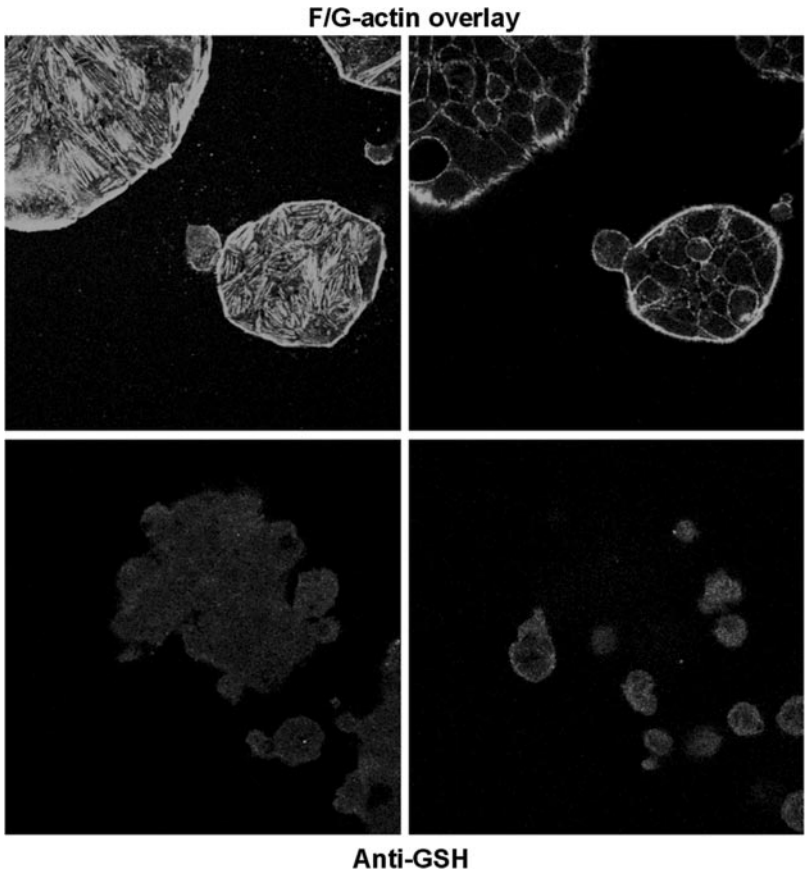

Fig. 8. Localization of F- and G-actin and of glutathionylated actin on PAPA NONOate (pNO) treatment in adherent cells. HT29-Cl.16E cells, cultured on glass coverslips, were treated for 48 h with 10^{-3} M pNO. Adherent cells were fixed and stained with Alexa 488-phalloidin (F-actin) and Texas red DNase I (G-actin). F- and G-actin overlay (*top*) of sectional images at the bottom (*left*) or top (*right*) of the clusters showed a normal stress fiber pattern of F-actin. Only rounded cells undergoing detachment at the periphery of the clusters showed depolymerized G-actin. Adherent cells were stained with an anti-reduced glutathione (*GSH*) antibody (*bottom*). Sectional images at the bottom (*left*) and top (*right*) of the clusters showed that rounded cells undergoing detachment at the periphery of the clusters were labeled.

pNO-treated cells. Concomitantly, using immunoblot analysis and immunofluorescence followed by confocal microscopy, we found an increase in glutathionylated actin compared with cells in the other phases of the cell cycle (data not shown). Finally, the entry into the G_2-M phase was associated with a dramatic increase in reduced glutathione without any major increase in GSSG (Table 1). As a consequence, the ratio GSH:GSSG was enhanced dramatically compared with cells in the other phases of the cell cycle.

pNO-Induced Apoptosis Is Caspase Independent. To reconcile these counterintuitive results (*i.e.,* apoptosis and thus activation of caspases, which are redox-active proteins on one hand and an oxidative stress on the other hand), one can raise the hypothesis that pNO-mediated apoptosis could be caspase independent. Thus, we examined DNA fragmentation, caspase-3 activation, and caspase-3 substrates cleavage.

When it came to characterizing DNA fragmentation, no internucleosomal degradation was found using conventional agarose gel electrophoresis in either adherent or floating cells after pNO treatment (Fig. 9*A*, *Lanes 2* and *3*, respectively). Interestingly, pulse field gel electrophoresis of DNA from floating cells disclosed a broad band corresponding to approximately 50–150 kb with a prominent fragment at 100 kb, which accounted for high molecular weight DNA fragmentation (Fig. 9*B, Lane 3*).

The synthetic peptide z-Val-Ala-Asp-fluoromethyl ketone (50 μM), a broad spectrum inhibitor of caspases, was unable to prevent cell detachment and cell death induced by NO (data not shown). In keeping with this finding, pNO treatment did not cause caspase-3 activation as shown by immunoblotting of floating cells (Fig. 10*A*, *Lane 2*). DFF45/ICAD is a caspase-3 substrate whose cleavage activates the endonuclease DFF40/CAD, leading to internucleosomal degradation of DNA (30, 31). In keeping with previous results, DFF45/ICAD was hardly detected on immunoblots of growing adherent cells treated with pNO (Fig. 10*B*, *Lane 1*; Ref. 18). Interestingly, DFF45/ICAD expression was restricted to pNO-treated floating cells and was not cleaved on pNO treatment (Fig. 10*B*, *Lane 2*). The absence of involvement of DFF45/ICAD in the apoptotic process correlates with (*a*) the absence of caspase-3 cleavage, and (*b*) the absence of internucleosomal DNA degradation. As a positive control in these immunoblot experiments, we used a treatment (IFN-γ, anti-Fas antibody, and Adriamycin referred to as IFA) leading to caspase-dependent apoptosis involving caspase-3 activation in HT29-Cl.16E cells. This treatment led to a typical DNA ladder (Fig. 9*A, Lane 4*) associated with caspase-3 cleavage (Fig. 10*A, Lane 4*) and disappearance of DFF45/ICAD (Fig. 10*B, Lane 4*).

We also looked at cytokeratin 18, another caspase-3 substrate, expressed in human gut epithelia and in a variety of human epithelial cell lines (32). The cleavage of cytokeratin 18 by caspase-3 generates an epitope that is specifically recognized by the M30 monoclonal antibody (28). As shown in Fig. 11, most cells released in the supernatant on pNO treatment scored negative with the M30 antibody, a finding in line with a caspase-independent cell death. In contrast, most cells released in the supernatant on IFA treatment scored positive for M30 antibody staining, a finding in agreement with the involvement of caspase-3 in this cell death.

Table 1 *Glutathione content of pNO-treated and control cells*[a]

The content of GSH and GSSG was assessed as described in "Materials and Methods." Results, expressed as nmole/mg protein, represent the mean ± SE of three determinations.

	GSH	GSSG	GSH/GSSG
pNO-treated cells			
Adherent cells	3.65 ± 0.08	0.37 ± 0.05	10.31 ± 1.47
Floating cells	23.3 ± 1.32	2.70 ± 0.17	8.65 ± 0.18
Control cells			
Adherent cells[b]	4.30 ± 0.05	0.41 ± 0.01	10.50 ± 0.32
G_2/M cells	17.80 ± 0.41	0.58 ± 0.04	30.98 ± 1.60

[a] pNO, PAPA NONOate; GSH, reduced glutathione; GSSG, oxidized glutathione.
[b] Refers to cells remaining adherent after vigorous shaking (see "Mitotic Detachment" in "Materials and Methods").

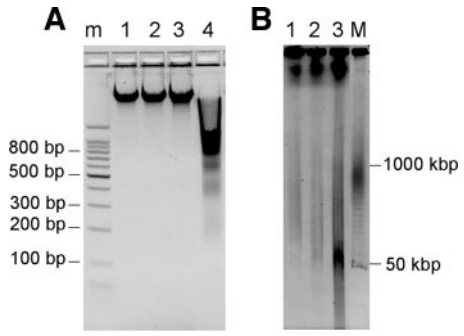

Fig. 9. DNA fragmentation on nitric oxide (NO) treatment. HT29-Cl.16E cells were treated or not with 10^{-3} M PAPA NONOate (pNO) for 48 h. *A*, conventional agarose gel electrophoresis. DNA extracted from untreated cells (*Lane 1*) or pNO-treated adherent or floating cells (*Lanes 2* and *3*, respectively) was analyzed in a 2% agarose gel stained with ethidium bromide (10 μg DNA/lane). DNA extracted from confluent HT29-Cl.16E cells submitted to IFA treatment (see "Materials and Methods") was used as a positive control for internucleosomal fragmentation (*Lane 4*). DNA size standard (*Lane M*) is indicated on the *left*. *B*, pulse field gel electrophoresis. Untreated cells (*Lane 1*) or pNO-treated adherent or floating cells (*Lanes 2* and *3*, respectively) were embedded in 0.75% agarose gel and subjected to pulse field gel electrophoresis in a 1% agarose gel as described in "Materials and Methods" (DNA of 0.5×10^6 cells per lane). DNA size standard (*Lane M*) is indicated on the *right*. Data shown are representative of two independent experiments.

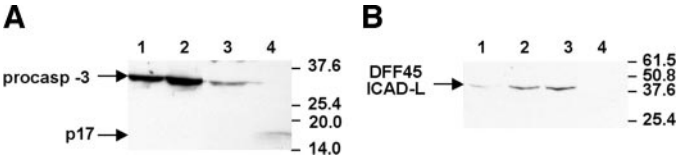

Fig. 10. Immunoblot analysis of caspase-3 and DFF45/ICAD-L on nitric oxide (NO) treatment. Caspase-3 (*A*) and DFF45/ICAD-L (*B*) immunoblots. HT29-Cl.16E cells were exposed to 10^{-3} M PAPA NONOate (pNO) or IFA treatment. Lysates obtained from adherent pNO-treated cells (*Lane 1*), floating pNO-treated cells (*Lane 2*), adherent IFA-treated cells (*Lane 3*), and floating IFA-treated cells (*Lane 4*) were submitted to SDS-PAGE electrophoresis as described in "Materials and Methods." *Numbers* on the *right* indicate molecular size of standards in kDa.

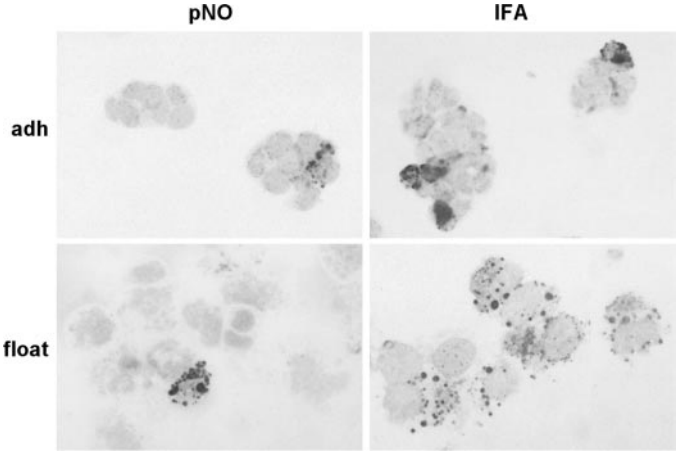

Fig. 11. Assessment of cytokeratin 18 cleavage on nitric oxide (NO) treatment. HT29-Cl.16E cells were exposed to 10^{-3} M PAPA NONOate (*pNO*) or IFA treatment. Adherent (*adh*) and floating cells (*float*) were immunostained with the M30 antibody (see "Materials and Methods"); original magnification, ×400.

DISCUSSION

This work is the first demonstration of a connection between the position of tumor cells in the cell cycle, their sensitivity to NO stress,

and their programmed cell death in relation with the cellular glutathione redox status. Of particular importance is the finding that NO, whatever its concentration (from 10^{-4} M to 10^{-3} M), exerted an early reversible cytostatic effect, attributed to ribonucleotide reductase inhibition, followed by the resumption of tumor cell progression into the cell cycle. However, this progression into the cell cycle led to late programmed cell death at the highest concentration of the NO donor pNO (10^{-3} M). Apoptotic cells accumulated in the G_2-M phase of the cell cycle as shown by flow cytometry, a finding that correlates well with the nuclear expression of cyclin B1, a cyclin specifically involved in the G_2-M transition, in cells undergoing detachment as shown by fluorescence microscopy (29). At that point of this study, it was important to determine whether inhibiting cell cycle entry was able to abrogate the programmed cell death. PD98059 is a potent blocker of cell entry in several cell types (33, 34) and in numerous cancer cell lines (35, 36), including HT29 cells (37). According to these previous studies, we found that treatment of HT29-Cl.16E cells with PD98059 led to an accumulation of cells into the G_0-G_1 phase of the cell cycle. We also found that PD98059 abrogated cell detachment and cell death, a finding showing that cell death on exposure to NO was caused by their entry into the cell cycle. Our finding reinforces this conclusion that confluent HT29-Cl.16E cells, mostly in the G_0-G_1 phase, are insensitive to NO treatment.

To decipher the molecular mechanisms underlying the sensitization of cycling cells to NO-related stress, we examined the cytoskeletal remodeling in connection with protein *S*-glutathionylation and GSH redox status during the G_2-M phase, in control conditions, and on NO treatment. In control cells, progression into the G_2-M phase was associated with actin depolymerization and its *S*-glutathionylation, together with the build-up of a high glutathione reducing power via a dramatic increase in GSH biosynthesis. Although the precise molecular mechanisms underlying actin *S*-glutathionylation during the G_2-M phase remain unclear, these results establish a connection between glutathione redox status and the cytoarchitectural changes during the G_2-M phase of the cell cycle.

Interestingly, several lines of investigations have shown that *S*-glutathionylation of actin is a reversible post-translational modification that prevents actin polymerization and stress fiber formation (38–40). In this context, G-actin glutathionylation would serve to maintain the cytoskeletal changes underlying the characteristic round morphology of the cells in the G_2-M phase. As after cytokinesis, stress fiber formation is required for daughter cells to reestablish contact with the extracellular matrix, it can be speculated that the build-up of a high GSH reducing power during G_2-M progression, which has been observed in other cell types (41) is the driving force for the process of deglutathionylation and actin repolymerization.

Experimental evidence of the past decade has demonstrated that changes in the ratio of GSH to GSSG may govern several important cellular functions, including apoptosis. Several lines of investigation have shown that on the effects of oxidative/nitrosative stresses, the GSH:GSSG ratio tends to decrease by increasing the concentration of GSSG (42). However, cells maintain glutathione redox state through the activation of the pentose phosphate pathway, which provides the reducing power in the form of NADPH required to recycle GSSG into GSH. On the basis of the manipulation of the carbohydrate content of culture media, we have shown that the cellular resistance of HT29-Cl.16E cells to a nitrosative stress is controlled by the carbon flux into the pentose phosphate pathway (16). In conditions of restricted carbon flux into the pentose phosphate pathway, most of the intracellular GSH is oxidized into GSSG within 1 h exposure to 10^{-3} M pNO and is associated with early cell death. Parallel cultures without limitation of the carbon flux into the pentose phosphate pathway (*i.e.*, culture in high glucose DMEM) maintain the redox status of GSH and survive the early cytotoxic effects of reactive nitrogen species. These findings support the concept that the metabolic adaptive response is essential for maintaining the glutathione redox status concomitantly with cell survival. In the present work, the absence of any change in the glutathione redox status in adherent cells on pNO treatment, compared with control cells, indicates that the reducing power required to maintain a constant glutathione pool in its reduced form does not exceed the cell metabolic adaptive response. Therefore, it is conceivable that the increase in the GSH pool during the G_2-M progression creates an oxidizable pool, which, on NO treatment, overwhelms the metabolic adaptive response and leads to a disruption of glutathione homeostasis. Together, our findings show that the dynamic balance of glutathione associated with the progression into the G_2-M phase is shifted toward an oxidized status on NO treatment.

S-Nitrosation of redox-active sites of caspases accounts for the protective effects of NO against caspase-dependent apoptosis (43, 44). Alternatively, high NO concentrations, which are sufficient to inhibit caspases, are able to induce a programmed cell death via a pathway independent of caspase activation (45–47). Interestingly, our results are in line with those previously reported by Xiang *et al.* (48), who have delineated a mechanism of programmed cell death in which blocking caspase activity did not prevent cell death. However, it prevented the cleavage of nuclear and cytoplasmic caspase substrates, whereas partial chromatin condensation still occurred (48). In HT29-Cl.16E cells, NO induced the cleavage of DNA into high molecular weight fragments, which were resolved as broad bands with a prominent fragment at approximately 100 kbp. In line with the concept that (*a*) caspase-3 is not necessary for high molecular weight DNA fragmentation (49), and (*b*) high molecular weight DNA fragmentation is all that is required for cells to complete apoptosis, including the nuclear features of apoptosis (49), we found that caspase-3 remained uncleaved on NO treatment.

In conclusion, based on a model of colonic cancer cells in culture, we have deciphered a mechanism of sensitization of cancer cells to programmed cell death that is dependent on the position of cells in the cell cycle. This important finding could help optimize anticancer treatments based on NO-donating compounds.

ACKNOWLEDGMENTS

We thank Dr. Caroline Colombeix for assistance with confocal microscopy and Dr. Nelly Robillard for help with flow cytometry. We also thank Marie Chedorge for technical assistance with electron microscopy. We thank Anne du Rusquet from the "Photologie" department for assistance.

REFERENCES

1. Lepoivre M, Flaman JM, Bobe P, Lemaire G, Henry Y. Quenching of the tyrosyl free radical of ribonucleotide reductase by nitric oxide. Relationship to cytostasis induced in tumor cells by cytotoxic macrophages. J Biol Chem 1994;269:21891–7.
2. Kim PK, Zamora R, Petrosko P, Billiar TR. The regulatory role of nitric oxide in apoptosis. Int Immunopharmacol 2001;1:1421–41.
3. Lee YJ, Lee KH, Kim HR, et al. Sodium nitroprusside enhances TRAIL-induced apoptosis via a mitochondria-dependent pathway in human colorectal carcinoma CX-1 cells. Oncogene 2001;20:1476–85.
4. Williams JL, Borgo S, Hasan I, Castillo E, Traganos F, Rigas B. Nitric oxide-releasing nonsteroidal anti-inflammatory drugs (NSAIDs) alter the kinetics of human colon cancer cell lines more effectively than traditional NSAIDs: implications for colon cancer chemoprevention. Cancer Res 2001;61:3285–9.
5. Millet A, Bettaieb A, Renaud F, et al. Influence of the nitric oxide donor glyceryl trinitrate on apoptotic pathways in human colon cancer cells. Gastroenterology 2002;123:235–46.
6. Kwon NS, Stuehr DJ, Nathan CF. Inhibition of tumor cell ribonucleotide reductase by macrophage-derived nitric oxide. J Exp Med 1991;174:761–7.
7. Guittet O, Ducastel B, Salem JS, et al. Differential sensitivity of the tyrosyl radical of mouse ribonucleotide reductase to nitric oxide and peroxynitrite. J Biol Chem 1998;273:22136–44.
8. Wink DA, Mitchell JB. Chemical biology of nitric oxide: insights into regulatory, cytotoxic, and cytoprotective mechanisms of nitric oxide. Free Radic Biol Med 1998;25:434–56.

9. Klein JA, Ackerman SL. Oxidative stress, cell cycle, and neurodegeneration. J Clin Invest 2003;111:785–93.
10. Chen QM, Liu J, Merrett JB. Apoptosis or senescence-like growth arrest: influence of cell-cycle position, p53, p21 and bax in H2O2 response of normal human fibroblasts. Biochem J 2000;347:543–51.
11. Chen QM, Merrett JB, Dilley T, Purdom, S. Down regulation of p53 with HPV E6 delays and modifies cell death in oxidant response of human diploid fibroblasts: an apoptosis-like cell death associated with mitosis. Oncogene 2002;21:5313–24.
12. Augeron C, Laboisse CL. Emergence of permanently differentiated cell clones in a human colonic cancer cell line in culture after treatment with sodium butyrate. Cancer Res 1984;44:3961–9.
13. Fogh J, Trempe G. New human tumor cells lines. In: Fogh J, editor. Human tumor cells in vitro: new human tumor cell lines. New York: Plenum Publishing Corp; 1975. p. 115–41.
14. Heerdt BG, Houston MA, Rediske JJ, Augenlicht LH. Steady-state levels of mitochondrial messenger RNA species characterize a predominant pathway culminating in apoptosis and shedding of HT29 human colonic carcinoma cells. Cell Growth Differ 1996;7:101–6.
15. Ho YS, Liu HL, Duh JS, et al. Induction of apoptosis by S-nitrosoglutathione and Cu2+ or Ni2+ ion through modulation of bax, bad, and bcl-2 proteins in human colon adenocarcinoma cells. Mol Carcinog 1999;26:201–11.
16. Le Goffe C, Vallette G, Jarry A, Bou-Hanna C, Laboisse CL. The in vitro manipulation of carbohydrate metabolism: a new strategy for deciphering the cellular defence mechanisms against nitric oxide attack. Biochem J 1999;344:643–8.
17. Velcich A, Corner G, Palumbo L, Augenlicht L. Altered phenotype of HT29 colonic adenocarcinoma cells following expression of the DCC gene. Oncogene 1999;18: 2599–606.
18. Charrier L, Jarry A, Toquet C, et al. Growth phase-dependent expression of ICAD-L/DFF45 modulates the pattern of apoptosis in human colonic cancer cells. Cancer Res 2002;62:2169–74.
19. Zhang M, Liu H, Guo R, et al. Molecular mechanism of gossypol-induced cell growth inhibition and cell death of HT-29 human colon carcinoma cells. Biochem Pharmacol 2003;66:93–103.
20. Bou-Hanna C, Berthon B, Combettes L, Claret M, Laboisse CL. Role of calcium in carbachol- and neurotensin-induced mucin exocytosis in a human colonic goblet cell line and cross-talk with the cyclic AMP pathway. Biochem J 1994;299:579–85.
21. Jarry A, Merlin D, Hopfer U, Laboisse CL. Cyclic AMP-induced mucin exocytosis is independent of Cl- movements in human colonic epithelial cells (HT29-Cl.16E). Biochem J 1994;304:675–8.
22. Merlin D, Augeron C, Tien XY, Guo X, Laboisse CL, Hopfer U. ATP-stimulated electrolyte and mucin secretion in the human intestinal goblet cell line HT29-Cl.16E. J Membr Biol 1994;137:137–49.
23. Merlin D, Guo X, Laboisse CL, Hopfer U. Ca2+ and cAMP activate different K+ conductances in the human intestinal goblet cell line HT29-Cl.16E. Am J Physiol 1995;268:C1503–11.
24. Ashihara T, Baserga R. Cell synchronization. Methods Enzymol 1979;58:248–62.
25. Tietze F. Enzymatic method for quantitative determination of nanogram amounts of total and oxidized glutathione: applications to mammalian blood and other tissues. Anal Biochem 1969;27:502–22.
26. Baker MA, Cerniglia G, Zaman A. Microtiter plate assay for the measurement of glutathione and glutathione disulfide in large numbers of biological samples. Anal Biochem 1990;190:360–5.
27. Solovyan V, Salminen A. A rapid and efficient method for preparation of genomic DNA suitable for analysis of both high and low molecular weight DNA fragmentation during neuronal apoptosis. Brain Res Protoc 1999;4:335–40.
28. Leers MP, Kolgen W, Bjorklund V, et al. Immunocytochemical detection and mapping of a cytokeratin 18 neo-epitope exposed during early apoptosis. J Pathol 1999;187:567–72.
29. Pines J, Hunter T. Cyclins A and B1 in the human cell cycle. Ciba Found Symp 1992;170:187–96.
30. Liu X, Zou H, Slaughter C, Wang X. DFF, a heterodimeric protein that functions downstream of caspase-3 to trigger DNA fragmentation during apoptosis. Cell 1997; 89:175–84.
31. Enari M, Sakahira H, Yokoyama H, Okawa K, Iwamatsu A, Nagata S. A caspase-activated DNase that degrades DNA during apoptosis, and its inhibitor ICAD. Nature 1998;391:43–50.
32. Caulin C, Salvesen GS, Oshima RG. Caspase cleavage of keratin 18 and reorganization of intermediate filaments during epithelial cell apoptosis. J Cell Biol 1997; 138:1379–94.
33. Meloche S, Seuwen K, Pages G, Pouyssegur J. Biphasic and synergistic activation of p44mapk (ERK1) by growth factors: correlation between late phase activation and mitogenicity. Mol Endocrinol 1992;6:845–54.
34. Squires MS, Nixon PM, Cook SJ. Cell-cycle arrest by PD184352 requires inhibition of extracellular signal-regulated kinases (ERK) 1/2 but not ERK5/BMK1. Biochem J 2002;366:673–80.
35. Fiddes RJ, Janes PW, Sivertsen SP, Sutherland RL, Musgrove EA, Daly RJ. Inhibition of the MAP kinase cascade blocks heregulin-induced cell cycle progression in T-47D human breast cancer cells. Oncogene 1998;16:2803–13.
36. Ukegawa JI, Takeuchi Y, Kusayanagi S, Mitamura K. Growth-promoting effect of muscarinic acetylcholine receptors in colon cancer cells. J Cancer Res Clin Oncol 2003;129:272–8.
37. Darmoul D, Gratio V, Devaud H, Lehy T, Laburthe M. Aberrant expression and activation of the thrombin receptor protease-activated receptor-1 induces cell proliferation and motility in human colon cancer cells. Am J Pathol 2003;162:1503–13.
38. Wang J, Boja ES, Tan W, et al. Reversible glutathionylation regulates actin polymerization in A431 cells. J Biol Chem 2001;276:47763–6.
39. Dalle-Donne I, Giustarini D, Rossi R, Colombo R, Milzani A. Reversible S-glutathionylation of Cys 374 regulates actin filament formation by inducing structural changes in the actin molecule. Free Radic Biol Med 2003;34:23–32.
40. Wang J, Tekle E, Oubrahim H, Mieyal JJ, Stadtman ER, Chock PB. Stable and controllable RNA interference: investigating the physiological function of glutathionylated actin. Proc Natl Acad Sci USA 2003;100:5103–6.
41. Soderdahl T, Enoksson M, Lundberg M, et al. Visualization of the compartmentalization of glutathione and protein-glutathione mixed disulfides in cultured cells. FASEB J 2003;17:124–6.
42. Hogg N, Singh RJ, Kalyanaraman B. The role of glutathione in the transport and catabolism of nitric oxide. FEBS Lett 1996;382:223–8.
43. Rossig L, Fichtlscherer B, Breitschopf K, et al. Nitric oxide inhibits caspase-3 by S-nitrosation in vivo. J Biol Chem 1999;274:6823–6.
44. Zech B, Kohl R, von Knethen A, Brune B. Nitric oxide donors inhibit formation of the Apaf-1/caspase-9 apoptosome and activation of caspases. Biochem J 2003;371: 1055–64.
45. Mohr S, McCormick TS, Lapetina EG. Macrophages resistant to endogenously generated nitric oxide-mediated apoptosis are hypersensitive to exogenously added nitric oxide donors: dichotomous apoptotic response independent of caspase 3 and reversal by the mitogen-activated protein kinase kinase (MEK) inhibitor PD 098059. Proc Natl Acad Sci USA 1998;95:5045–50.
46. Okuno S, Shimizu S, Ito T, et al. Bcl-2 prevents caspase-independent cell death. J Biol Chem 1998;273:34272–7.
47. Kim YM, Chung HT, Simmons RL, Billiar TR. Cellular non-heme iron content is a determinant of nitric oxide-mediated apoptosis, necrosis, and caspase inhibition. J Biol Chem 2000;275:10954–61.
48. Xiang J, Chao DT, Korsmeyer SJ. BAX-induced cell death may not require interleukin 1 beta-converting enzyme-like proteases. Proc Natl Acad Sci USA 1996;93: 14559–63.
49. Walker PR, Leblanc J, Carson C, Ribecco M, Sikorska M. Neither caspase-3 nor DNA fragmentation factor is required for high molecular weight DNA degradation in apoptosis. Ann N Y Acad Sci 1999;887:48–59.